Amidation modified waste polystyrene foam as an efficient recyclable adsorbent for organic dyes removal

Yanghao Pu, Zhengfeng Xie, Hao Ye and Wei Shi

ABSTRACT

Modifying environmentally harmful waste polystyrene foam as an efficient recyclable adsorbent for organic dyes is important. Amidation modified polystyrene (PS-SD) was prepared by the Friedel-Crafts reaction and N,N′-dicyclohexylcarbodiimide (DCC) dehydration condensation reaction of waste polystyrene foam. PS-SD had highly efficient removal performance for organic dyes in large volume water sample solutions, and equilibrium was achieved in 0.5 h. The maximum adsorption capacities for Methylene blue (MB) and Congo red (CR) were 881.62 and 1,880.91 mg/g, respectively, at room temperature according to the Langmuir adsorption isotherm ($R^2 > 0.99$). The kinetic data of the two dyes followed pseudo-second-order kinetics. The removal percentage remained high (>85%) after eight filtration-regeneration cycles. Experimental results showed that PS-SD was an excellent adsorbent for water treatment with high recyclability and long life.

Key words | adsorption, amidation, organic dyes, recyclability, waste polystyrene foam

HIGHLIGHTS

- Modification of waste materials.
- The reusability, and high adsorption capacity of amidated PS-SD.
- High value-added products, which can be used for wastewater treatment.

GRAPHICAL ABSTRACT

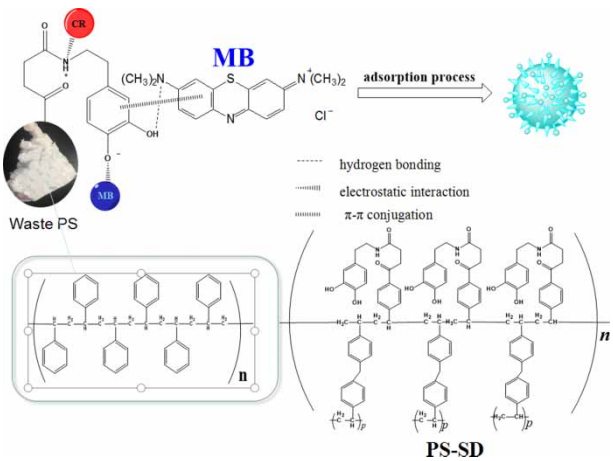

Yanghao Pu
Oil & Gas Field Applied Chemistry Key Laboratory of Sichuan Province, College of Chemistry and Chemical Engineering,
Southwest Petroleum University,
Chengdu 610500,
China

Zhengfeng Xie (corresponding author)
Oil & Gas Field Applied Chemistry Key Laboratory of Sichuan Province, College of Chemistry and Chemical Engineering, Southwest Petroleum University,
Research Institute of Industrial Hazardous Waste Disposal and Resource Utilization, Southwest Petroleum University,
Chengdu 610500,
China
E-mail: *xiezhf@swpu.edu.cn*

Hao Ye
Wei Shi
College of Chemistry and Chemical Engineering,
Southwest Petroleum University,
Chengdu 610500,
China

doi: 10.2166/wst.2021.129

INTRODUCTION

Considerable organic dye wastewater is discharged directly without treatment, which has caused a sharp increase in the types and content of existing pollutants in water bodies (Chan *et al.* 2016; Wang *et al.* 2018b; Cheng *et al.* 2019; Roy *et al.* 2019). These pollutants are often complex, highly toxic, and difficult to degrade; thus, they are gradually accumulated. Through the food chain, such pollutants cause great pollution to the ecological environment and biosphere, and restrict the sustainable development of harmonious coexistence between human and nature (Han *et al.* 2019; Choi *et al.* 2020; Dinari *et al.* 2020; Lei *et al.* 2020). Therefore, removal of organic dyes from wastewater has become important for the environment (Cho *et al.* 2018; Wang *et al.* 2020). However, cationic dye Methylene blue (MB) and anionic dye Congo red (CR) are common organic dyes (Wan *et al.* 2017; Ma *et al.* 2020).

At present, biodegradation, photocatalysis, and flocculation can effectively remove dyes in wastewater (Liu *et al.* 2018; Unnikrishnan *et al.* 2018; Wang *et al.* 2018a; Naushad *et al.* 2019; Satheshkumar *et al.* 2020; Sharma *et al.* 2020). However, these methods usually have complex process flows, high operating costs, and high energy consumption. By contrast, adsorption has become a research hotspot in recent years because of its simple operation, large processing capacity, easy design and operation, and low cost (Naushad *et al.* 2015; Duan *et al.* 2019).

At present, domestic and foreign researchers have conducted several studies on the resource utilisation of waste polystyrene foam (Dardouri *et al.* 2018). Polystyrene has a three-dimensional network structure, which has a certain good effect on adsorption. A novel amino modified hierarchically macro–mesoporous cross-linked polystyrene adsorbent (HP CLPS-EDA) was fabricated via the combination of colloidal crystal templating with the Friedel-Crafts (F-C) technique, and the adsorption performance of salicylic acid from aqueous solutions on HP CLPS-EDA was investigated (Zhang *et al.* 2018a). A novel hybrid nanomaterial was fabricated by encapsulating chitosan molecules (CS) into charged polystyrene resin (PS) through electrostatic adsorption. The resulting hybrid absorbent (PS-CS) demonstrates highly efficient sorption towards cupric ion (Liu *et al.* 2019b). However, research on the use of waste polystyrene adsorption is limited. A conjugated microporous polymer (CMP) was synthesised using post-consumer waste polystyrene (WPS) and activated into a resin with sulfonic acid groups (SCMP). The maximum adsorption capacity of CR for CMP and SCMP was 500 and 357 mg/g, respectively (Chaukura *et al.* 2017).

The removal of MB and CR from wastewater is important. To date, some researchers have prepared highly effective adsorbents for the adsorption of MB and CR (Albadarin *et al.* 2017; Daneshvar *et al.* 2017; Ahmed *et al.* 2020). It provides ideas for studying the adsorption materials of MB and CR. Therefore, we will synthesise a series of new dye adsorbents that are highly efficient, stable, and reusable. In this paper, PS-SD was synthesised from dopamine and carboxylated waste polystyrene, which was prepared by the Friedel-Crafts reaction of waste polystyrene foam and succinic anhydride. Waste polystyrene foam is easily soluble in dichloromethane. The reaction conditions are efficient and simple. This work will provide a novel way to recycle waste polystyrene materials into high value-added products that can be used for wastewater treatment. Using CR and MB as model pollutants, the adsorption characteristics of amide-functionalised polystyrene adsorbents are studied. The amount of adsorbent, pH value, temperature, time, and initial dye concentration (C_0) during adsorption have been well studied and optimised. The main objectives of this work are as follows: to study the feasibility of using the modified PS as an adsorbent to remove CR and MB, to determine the applicability of various isotherm models (Langmuir and Freundlich) and find the best-fitting isotherm equation, to evaluate the kinetic parameters and explain the adsorption properties, and to compare PS-SD with other adsorbents.

EXPERIMENTAL SECTION

Materials

Waste polystyrene foam was obtained from a reagent packaging box. Dopamine hydrochloride (DA) (98%) was purchased from Aladdin, China. Other materials such as succinic anhydride and N,N''-dicyclohexylcarbodiimide (DCC) were purchased from Adamas Chemical Reagent Factory (Shanghai, China). Dichloromethane (CH_2Cl_2) was purchased from Kelong Chemical Reagent Factory (Chengdu, China). MB and CR were of analytical grade and purchased from Adamas Chemical Reagent Factory (Shanghai, China).

Preparation of modified PS-SD

The carboxyl group was grafted onto waste polystyrene foam by the Friedel-Crafts reaction to obtain carboxylated polystyrene (PS-S). 0.01 mol of PS-S, 0.01 mol of dopamine, and 0.01 mol of DCC were added to a round-bottomed flask containing 35 mL of dichloromethane and stirred at room temperature for 12 h. Then 20 mL of deionised water was added, and the solid was washed with dichloromethane, ethanol, and deionised water to obtain PS-SD. The reaction scheme is shown in Figure 1.

Effect of solution pH on adsorption

The acidity and alkalinity of the adsorption system are important factors for studying the mechanism of adsorption, which can affect the adsorption of different electrical dyes. CR and MB were selected as ionic dyes for experiments. MB and CR solutions were prepared with a concentration of 100 mg/L. The pH of MB and CR solutions was adjusted by 1.0 mol/L of NaOH and 1.0 mol/L of HCl aqueous solution to investigate the effect of pH on adsorption for MB and CR. Ten milligrams of PS-SD was added directly into a 20 mL glass bottle containing 10 mL of MB and CR solutions (100 mg/L), which was treated by ultra-sonication for 10 min and shaken at 200 rpm in a water bath at 298.15 K for 150 min. The experiment was repeated three times. The pH range of the dye solution was adjusted to 2–12. The adsorption capacity of the PS-SD for dyes can be calculated using the following formula (Wan *et al.* 2017):

$$q_e = \frac{V(C_0 - C_e)}{m} \quad (1)$$

where C_0 is the initial dye concentration (mg/L), C_e is the dye concentration in solution (mg/L) at equilibrium, V is the volume of the solution (L), and m is the mass of the adsorbent (g).

Effect of initial concentration on adsorption

The static adsorption experiment was performed in a volumetric flask, and 10 mg of the modified PS samples was added to MB (the concentration range was 50–1,000 mg/L) and CR (the concentration range was 50–2,500 mg/L) solutions. Adsorption was performed by shaking in a water

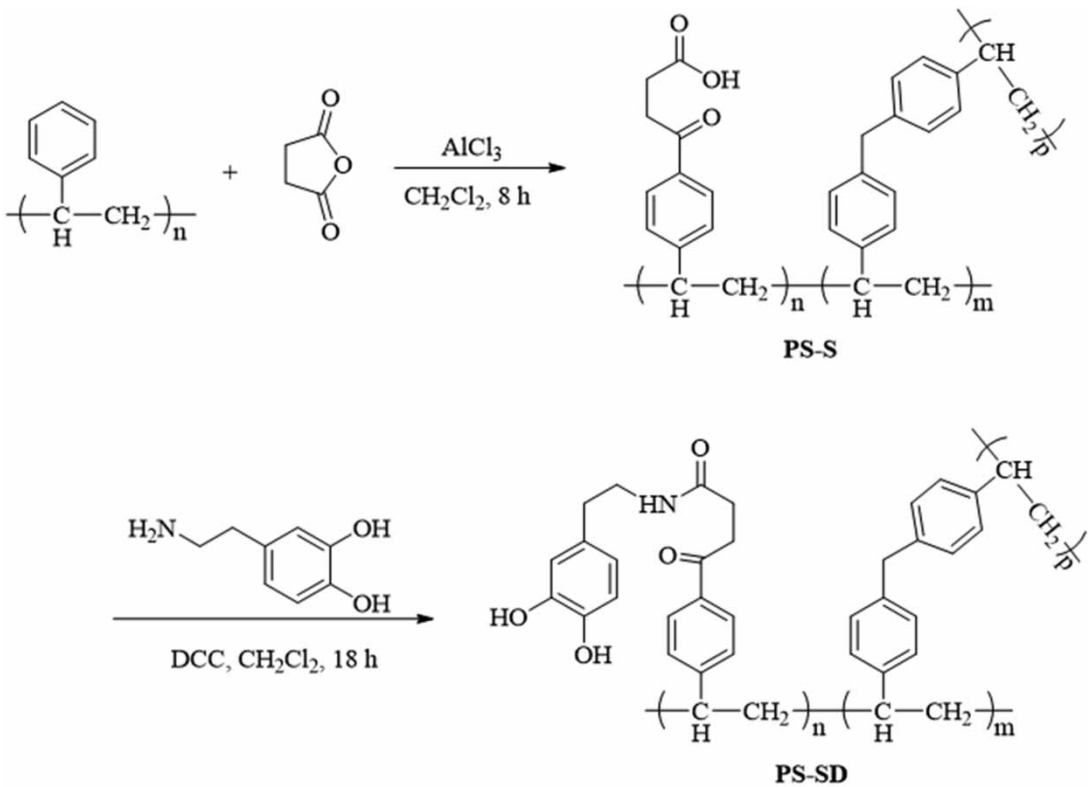

Figure 1 | Schematic diagram of amide modification reaction.

bath (200 rpm) at 298.15 K. The experiment was repeated three times. According to the pre-established calibration curve, the concentration of MB and CR in the aqueous solution was analysed at 665 and 497 nm, respectively, using an ultraviolet spectrophotometer. The Langmuir adsorption isotherm model and Freundlich adsorption isotherm model were used to simulate the experimental data. The Langmuir equation is as follows (Tran *et al.* 2017):

$$q_e = \frac{q_m \cdot K_L \cdot C_e}{1 + K_L \cdot C_e} \tag{2}$$

where q_m (mg/g) is the maximum saturated monolayer adsorption capacity of an adsorbent, q_e (mg/g) is the amount of adsorbate uptake at equilibrium, and K_L (L/mg) is a constant related to the affinity between an adsorbent and adsorbate.

The Freundlich equation is as follows (Qiao *et al.* 2020):

$$q_e = K_F \cdot C_e^{1/n} \tag{3}$$

where q_e (mg/g) is the amount of adsorbate uptake at equilibrium, K_F (mg/g)/(mg/L)^n is the Freundlich constant, and n (dimensionless) is the Freundlich intensity parameter.

Effect of contact time on adsorption

The adsorption kinetics experiment determines the mechanism and potential rate control step of adsorption by analysing the change trend of the adsorption capacity over time. The adsorption kinetics experiments were conducted by adding 10 mg of PS-SD into a 20 mL glass bottle containing 10 mL of MB and CR solutions with a concentration of 100 mg/L. Adsorption was performed by shaking in a water bath (200 rpm) at 298.15 K. The experiment was repeated three times. The pseudo-first-order equation and pseudo-second-order equation in the diffusion model were used to fit the experimental data to nonlinear adsorption.

The pseudo-first-order equation is as follows (Ji *et al.* 2020):

$$\ln(q_e - q_t) = \ln q_e - k_1 t \tag{4}$$

where q_e and q_t are the amounts of adsorbate uptake per mass of adsorbent at equilibrium and at any time t (min), and k_1 (1/min) is the rate constant of the PFO equation.

The pseudo-second-order kinetic model refers to the linear relationship between the reaction rate and the concentration of the two reactants. The rate control step of adsorption was the interaction between the adsorbate and the adsorption site on the adsorbent surface, which was expressed as the equation (Wu *et al.* 2019):

$$\frac{t}{q_t} = \frac{1}{k_2 q_e^2} + \frac{1}{q_e} t \tag{5}$$

where k_2 (1/min) is the rate constant of the PSO equation.

Effect of solution temperature on adsorption

Thermodynamic experiments were conducted by adding 10 mg PS-SD into a 20 mL glass bottle containing 10 mL of MB and CR solutions with concentrations of 1,000 and 2,500 mg/L, respectively. At this concentration, the maximum adsorption capacity was reached. Adsorption was performed by shaking in a water bath (200 rpm) at 298.15, 308.15, and 318.15 K. The experiment was repeated three times. The thermodynamic parameters, including Gibbs free energy change value (ΔG^{θ}), enthalpy change (ΔH^{θ}), and entropy change (ΔS^{θ}), were calculated using the Van't Hoff formula, which can describe the adsorption mechanism. The Van't Hoff formula is as follows (Gao *et al.* 2019):

$$\begin{aligned} \ln K_a &= \frac{\Delta S^{\theta}}{R} - \frac{\Delta H^{\theta}}{R \cdot T} \\ K_a &= \frac{q_e}{C_e} \\ \Delta G^{\theta} &= \Delta H^{\theta} - T \cdot \Delta S^{\theta} \end{aligned} \tag{6}$$

where R is the universal gas constant (8.3144 J/(mol × K)) and T is the absolute temperature in Kelvin.

Characterisation

The resulting materials were characterised by Fourier transform infrared (FTIR, WQF-520) spectroscopy between 4,400 and 400 cm^{-1} using the KBr pellet technique. Scanning electron microscopic (SEM) images were obtained on a field emission scanning electron microscope (THS-112). Nitrogen adsorption/desorption isotherm was measured at 77 K with Autosorb- 1 (Quantachrome, USA). The specific surface area was calculated by the Brunauer-Emmett-Teller (BET) equation using the adsorption data at relative pressure of 0.05–0.3. Thermogravimetric analysis (TGA) of PS-S and PS-SD was performed using a SDTA851 (METTLER, Switzerland) thermo-gravimetric analyser

under N_2 atmosphere at a heating rate of 10 °C min^{-1} from 40 to 700 °C.

RESULTS AND DISCUSSION

Characterisation of PS-SD

FTIR analysis was performed to explore the surface properties of PS-S and PS-SD, and the spectrum is presented in Figure 2. In Figure 2(b), the peak at 3,450 cm^{-1} was attributed to the stretching vibration of the O-H bond and the peak at 1,680 cm^{-1} was assigned to stretching vibration of the C = O bond (Liu *et al.* 2020b). In Figure 2(c), the peaks at 3,400 and 1,640 cm^{-1} were related to the N-H and C = O bonds in the amide group.

Nitrogen adsorption–desorption isotherms of PS-SD before and after adsorption of MB and the pore size distributions of samples are compared in Figure 3. The specific surface area was calculated from the N_2 adsorption isotherm by using the Branauer-Emmett-Teller (BET) model, and the pore size distribution was determined by using the Barrett-Joyner-Halenda (BJH) model. PS-SD showed a typical H4 hysteresis loop and the isotherm belonged to type IV (Duan *et al.* 2019). The adsorption capacity of PS-SD dropped sharply after MB adsorption because of the MB molecules at the adsorption sites; thus, the BET surface area of PS-SD declined from 21.63 to 5.84 $m^2 g^{-1}$ during adsorption. The result indicated that PS-SD had an abundant mesoporous structure, as further confirmed by the pore size distribution. The pore size of PS-SD ranged from 1.46 to 140 nm with a peak value at a pore diameter of 20 nm.

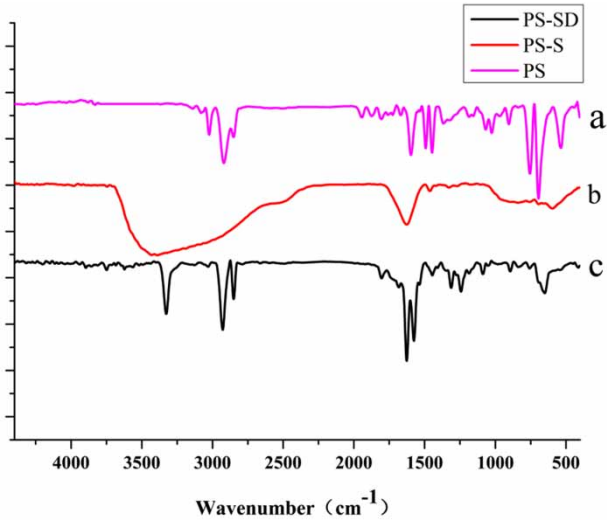

Figure 2 | FTIR spectra of PS (a), PS-S (b), PS-SD (c).

The thermal decomposition of PS-SD was investigated and compared with that of PS and PS-S (Figure 4). The total mass of PS-S and PS-SD gradually decreased with the increase of temperature. We have considered the weight losses of 2–6% at 200 °C insignificant, as the evaporation of solvent and/or water molecules was retained in the polymer chains. However, a big difference in mass loss occurred between PS-S and PS-SD before reaching 350 °C, which was primarily due to the volatilization of the pyrolysis of the oxygen-containing functional groups (Wang *et al.* 2019). The serious weight loss of PS-SD in this stage demonstrated the occurrence of several defects and oxygen-containing functional groups including amide and hydroxyl groups in PS-SD. A pure PS sample showed weight loss with its onset at approximately 350 °C. After reaching 350 °C, rapid mass loss rates of PS, PS-S, and PS-SD occurred at approximately 430 °C, which were due to decarbonisation of the polystyrene matrix. These results demonstrated that PS, PS-S, and PS-SD polymers had good thermal stability. The thermal degradation of PS-SD indicated that amidation modification had been completed.

The microstructures of the as-prepared products were characterised from their SEM images. Figure 5 shows representative SEM images of PS and PS-SD. Polystyrene had a smooth surface. After amidation modification, the surface was fluffy and porous, which was suitable for adsorption. As shown in Figure 5(c) and 5(d), after MB was adsorbed, the pores were occupied, and MB molecules were found on the surface. This result indicated that adsorption was consistent with physical adsorption and chemical adsorption.

Effect of solution pH on adsorption

Solution pH played an important role in adsorption because it strongly influenced the binding sites of the adsorbent. As shown in Figure 6, the adsorption capacity of CR increased and then decreased with the increase of pH. Under acidic conditions, the amino group of the modified PS was protonated to form $-NH_3^+$, which combined with the anionic CR through electrostatic interaction. When the pH value was relatively low (pH < 4), H^+ combined with the sulfonic acid group of CR, and the electronegativity of CR was weakened. The electrostatic attraction between the adsorbent and CR was reduced. The adsorption capacity of MB gradually increased with the increase of pH. Under alkaline conditions, the phenolic hydroxyl of modified PS was combined with cationic MB through hydrogen bond interaction (Wan *et al.* 2017; Lin *et al.* 2019). The adsorption of MB on the PS-SD surface generally followed an ionic interaction

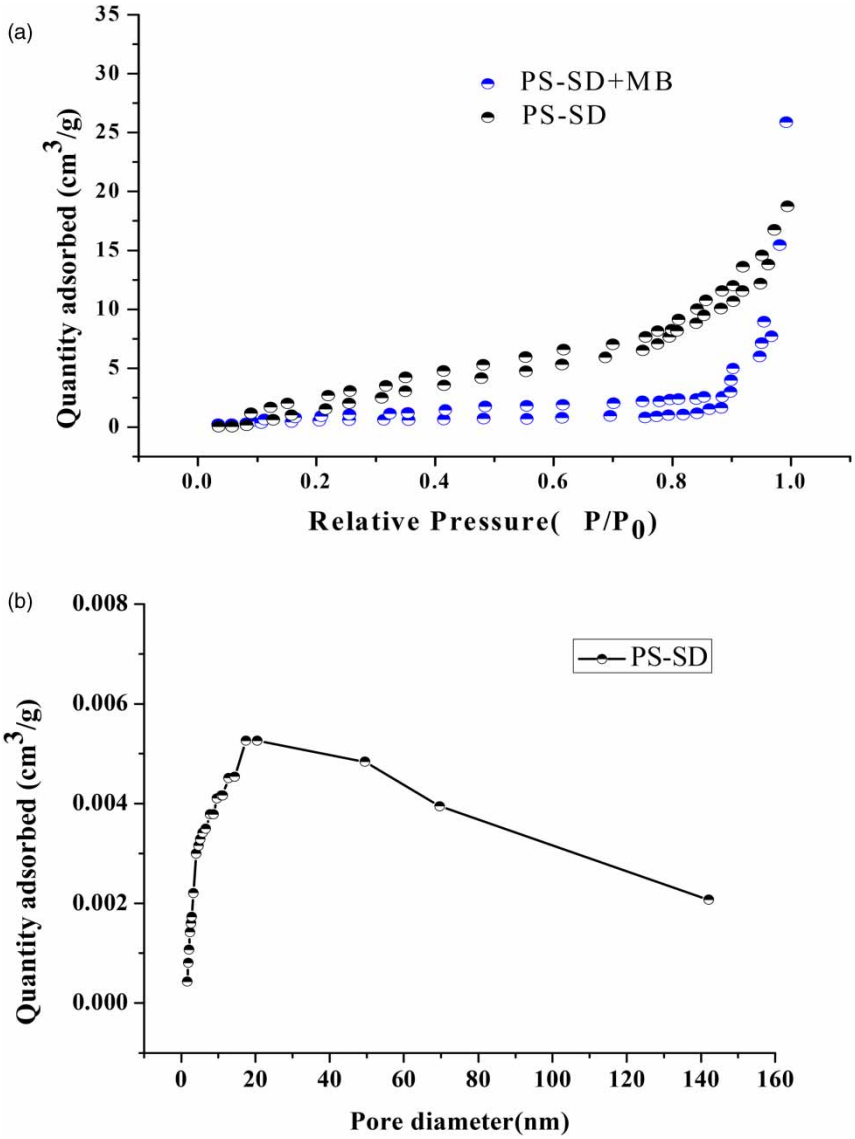

Figure 3 | (a) Nitrogen adsorption isotherms of PS-SD before and after the adsorption of MB, (b) BJH pore size distribution desorption curve of PS-SD.

mechanism in which the surface charge of the adsorbent determined the type of interactions between the binding sites of the adsorbent and the adsorbate molecules. When pH = 9, the surface of the adsorbent was already positively charged, and electrostatic repulsion was observed between the adsorbent and the dye molecules. However, PS-SD still had high adsorption performance for CR at this time, indicating the occurrence of other adsorption mechanisms apart from electrostatic interaction. Under natural conditions, the adsorption effect of modified PS-SD on anionic dyes was higher than that on cationic dyes (Lin *et al.* 2019).

Isotherm studies

The adsorption isotherm model fitting results of the amide modified waste polystyrene PS-SD for CR and MB dyes are shown in Figures 7 and 8, respectively, and the fitting parameters are shown in Table 1. R^2 (0.99, 0.93) of MB and CR by Langmuir was higher than R^2 (0.88, 0.55) of MB and CR by Freundlich. This finding indicated that adsorption can be better described by the Langmuir adsorption isotherm model. These results showed that adsorption occurred at specific homogeneous sites within the adsorbent, indicating a monolayer coverage

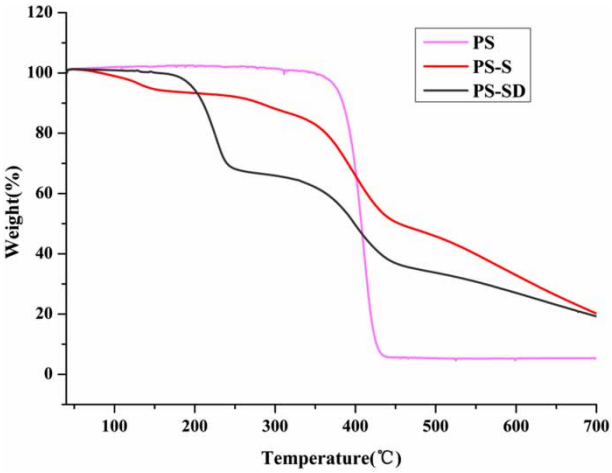

Figure 4 | TGA curves of PS (a), PS-S (b), PS-SD (c).

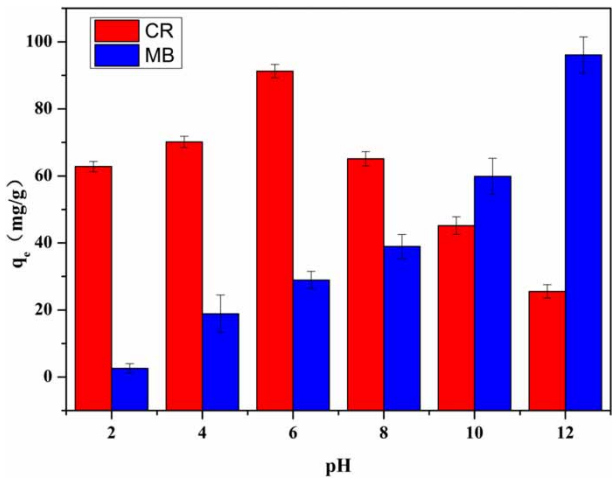

Figure 6 | Effect of different pH on the adsorption capacity of CR and MB (dosage of absorbent = 10 mg, C_0 = 100 mg/L, t = 150 min, T = 298.15 K).

adsorption mechanism (Li *et al.* 2019). The maximum adsorption capacity of the modified PS on CR and MB can be calculated using the fitting equation as 1,880.91 and 881.62 mg/g, which were different from the actual measurement of 1,862.18 and 863.74 mg/g, respectively. Remarkably, the maximum adsorption capacities were much higher than the values obtained in previously reported adsorbents. Compared with most hydrogels, carbon materials, and other adsorbents reported in Table 2, PS-SD showed excellent MB and CR adsorption capacity.

In addition, n calculated by the Freundlich model equation was in the range of 1–10, revealing that CR and MB adsorption onto the absorbent was favorable adsorption.

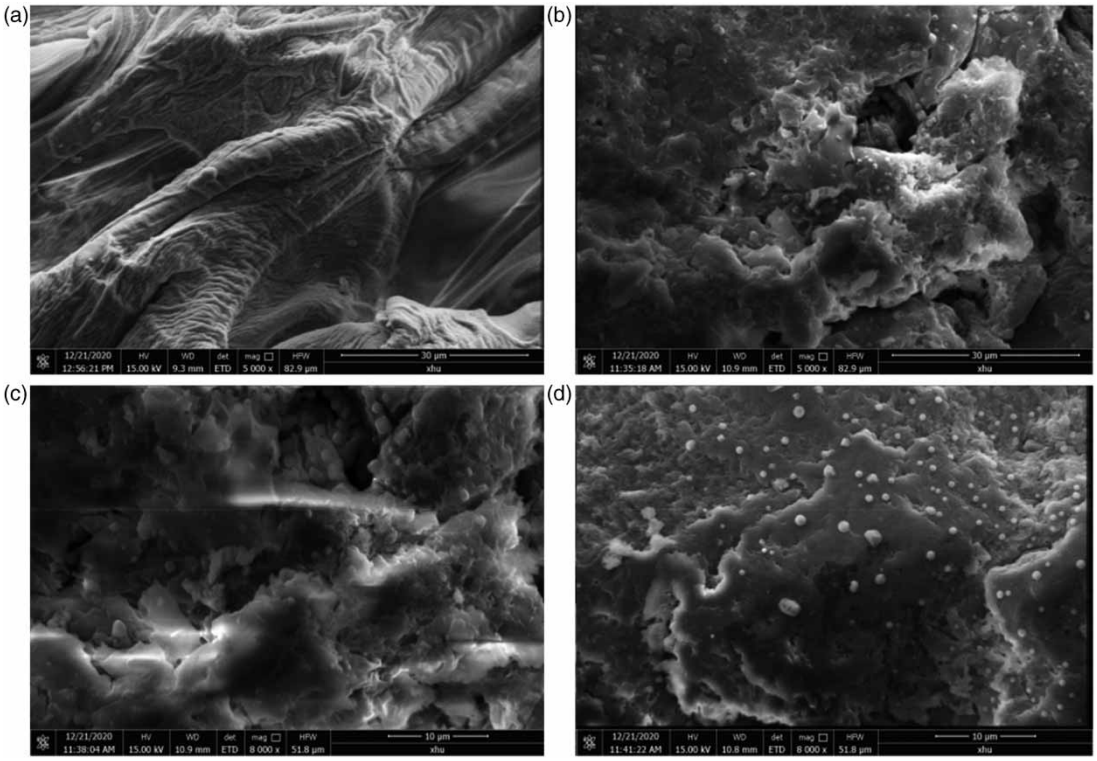

Figure 5 | SEM images of PS (a), PS-SD (b) and (c), PS-SD after the adsorption of MB (d).

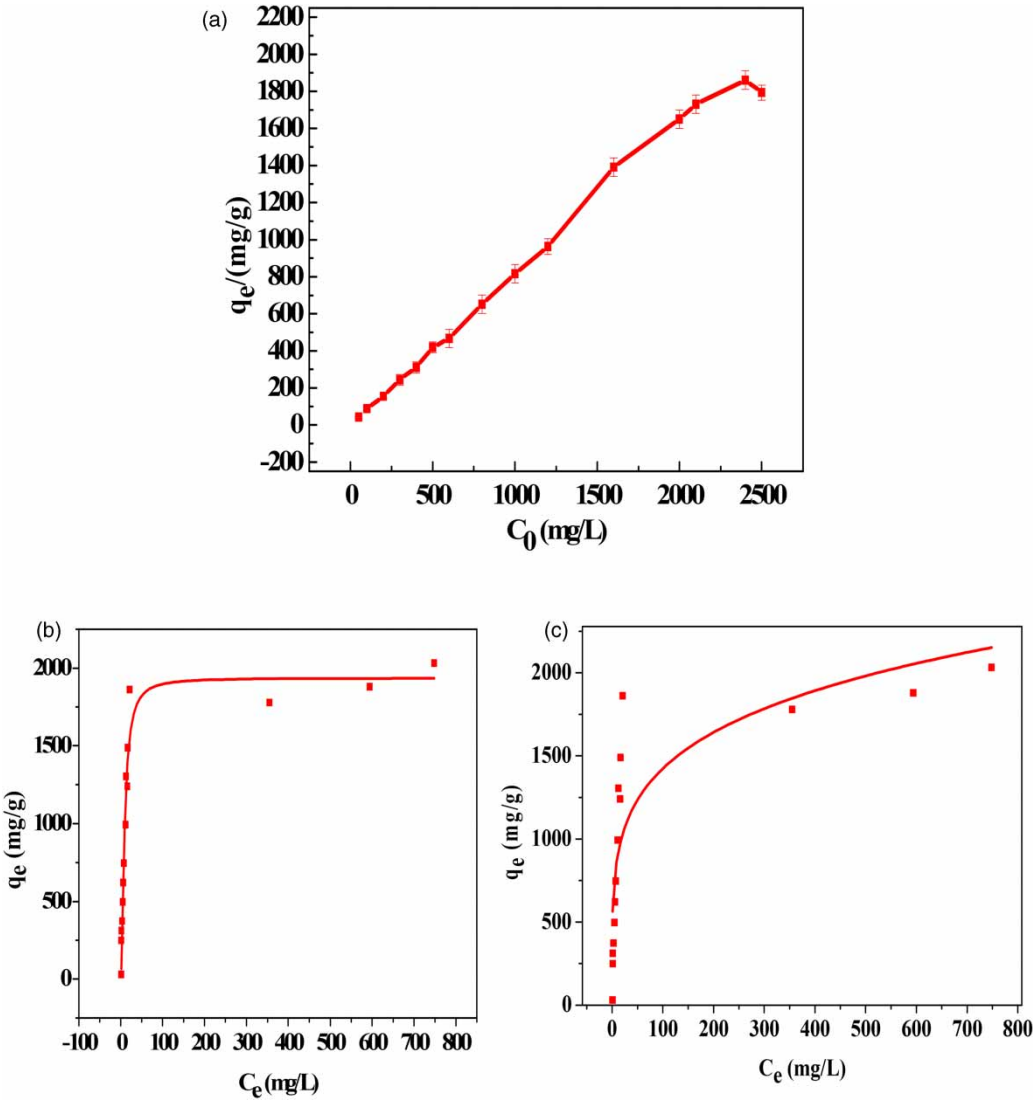

Figure 7 | (a) The effect of initial concentration on the adsorption of CR by PS-SD adsorbent (dosage of absorbent = 10 mg, C_0 = 50–2,500 mg/L, t = 150 min, T = 298.15 K, pH = 5). (b) Langmuir, (c) Freundlich.

Kinetic studies

The adsorption capacity and first-order and second-order kinetics of the amidated modified polystyrene PS-SD with adsorption time of 150 min are shown in Figure 9. Within 10 min of the beginning of adsorption, the amidated modified polystyrene PS-SD had a fast adsorption rate for dyes, and the adsorption capacity increased rapidly and reached saturation adsorption (Xi *et al.* 2020). In the initial stage of adsorption, the surface activity adsorption sites of the modified polystyrene PS-SD were abundant, and a large number of cavities appearing on the surface of the particles after amide modification were not completely occupied by dye molecules, which made dye adsorption PS-SD easy (Liu *et al.* 2020a). When the adsorption time continued to extend, the active adsorption sites on the surface of the adsorbent and the inner surface of the cavity were largely occupied by dye molecules (Wan *et al.* 2017). Similarly, as adsorption progressed, the dye concentration in the solution decreased, and the concentration driving force was not conducive for adsorption. The adsorption rate decreased, and the adsorption capacity did not increase after 30 min; the adsorption equilibrium state was basically reached (Wu *et al.* 2020). As shown in Figure 9(b) and 9(c), the fitting degree of the pseudo-second order kinetic model was better than that of the pseudo-first order kinetic model, which was supported by the correlation coefficient shown in Table 3. For instance, the correlation coefficient R^2 from the pseudo-first order kinetic model of MB and CR was

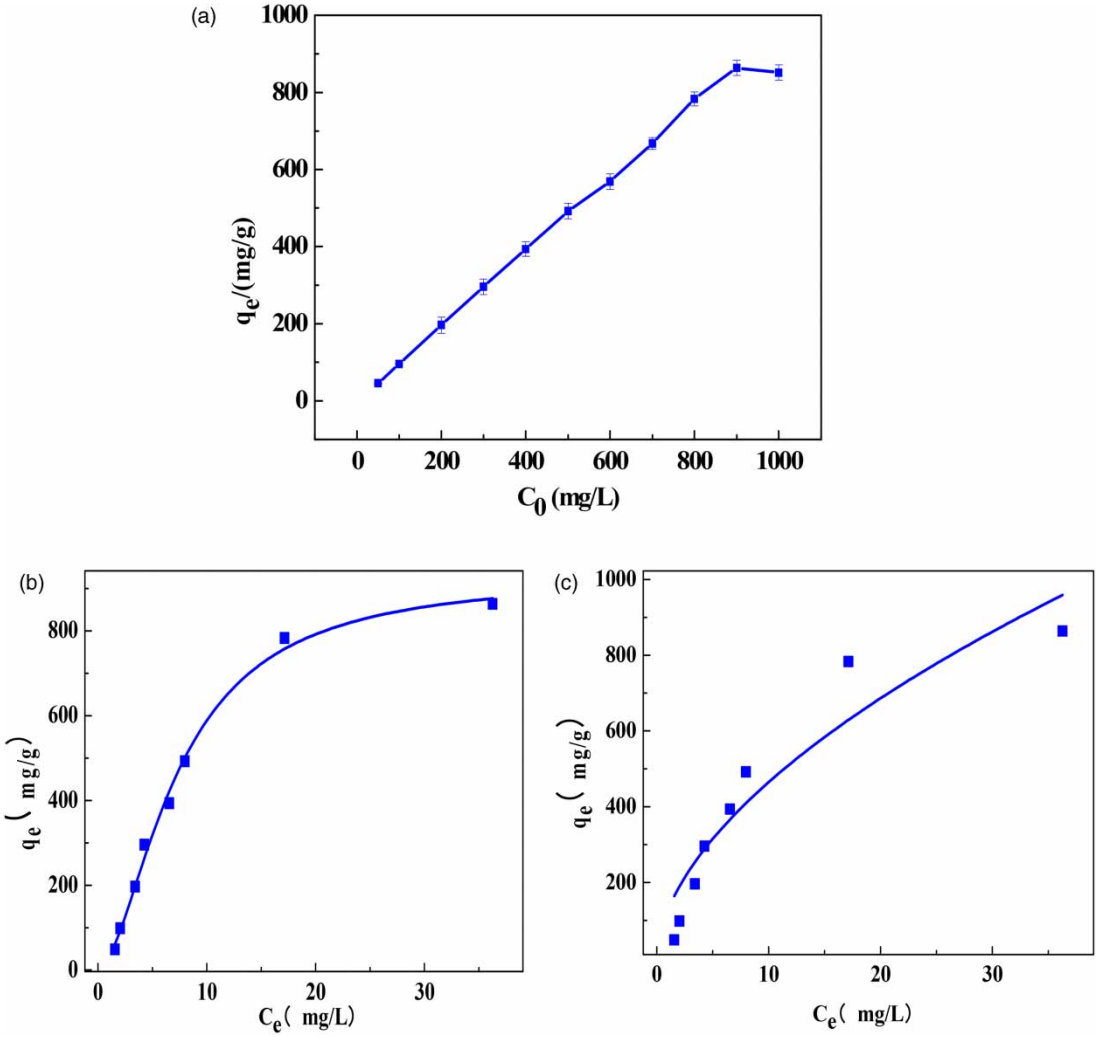

Figure 8 | (a) The effect of initial concentration on the adsorption of MB by PS-SD adsorbent (dosage of absorbent = 10 mg, C_0 = 50–1,000 mg/L, t = 150 min, T = 298.15 K, pH = 10). (b) Langmuir, (c) Freundlich.

Table 1 | Isotherm constants and values of CR and MB adsorption using PS-SD

Isotherm model	Parameter	CR	MB
Langmuir	q_m(cal)	1,880.91	881.62
	q_m(exp)	1,862.18	863.74
	K_L	0.026	0.03
	R^2	0.93	0.99
Freundlich	K_F	547.72	127.32
	n	4.20	1.79
	R^2	0.55	0.88

The temperature of experiments is 298.15 K.

only 0.64 and 0.53, which were lower than those of the pseudo-second order model ($R^2 \geq 0.995$). In addition, the experimental values of q_e were in close agreement with the values calculated by using the pseudo-second order model, whereas the experimental values of q_e differed largely from the calculated values obtained by the pseudo-first order model. This finding implied that the pseudo-second order model was suitable to describe the kinetic behaviours of MB and CR onto PS-SD. Therefore, the PS-SD adsorption rate was susceptible to chemical adsorption, and chemical adsorption might be one of the rate control steps in adsorption process (Li *et al.* 2020).

Effect of solution temperature

The different thermodynamic parameters of adsorption could determine its spontaneity, randomness, endothermicity or exothermicity. Figure 10 shows the equilibrium adsorption capacity of MB and CR by modified polystyrene PS-SD at 298.15, 308.15, and 318.15 K. Table 4 shows that ΔH^{θ} was always positive during adsorption, which indicated

Table 2 | Adsorption capacities of various adsorbents for the removal of dyes

Adsorbents	Dye	Isotherm model	q(mg/g)	References
r GO-IO composites	MB	Langmuir	39	Sharif *et al.* (2017)
GHA gels	MB	Langmuir	55.9	Cui *et al.* (2015)
Graphene gel	MB	Langmuir	334.5	Lau *et al.* (2018)
Crosslinked cellulose dialdehyde	CR	Langmuir	42.03	Kumari *et al.* (2016)
Functionalised carbon nanotube/mixed	CR	Langmuir	1,250	Yang *et al.* (2015)
Brown macroalga	MB	Langmuir	95.45	Daneshvar *et al.* (2017)
Modified PS-SD	MB CR	Langmuir	881.62 1,880.91	This work

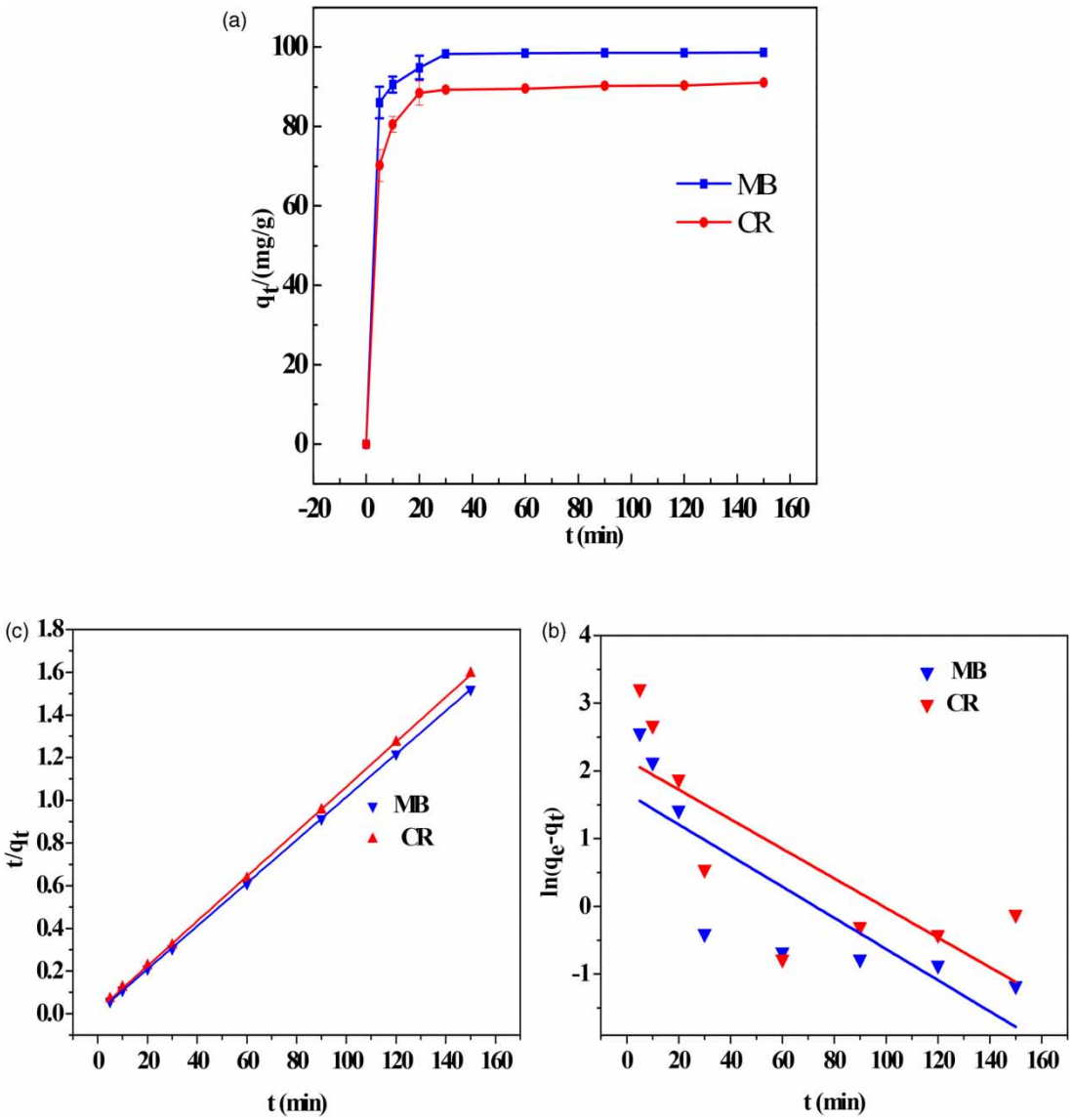

Figure 9 | (a) Effect of contact time on the CR and MB adsorption using the PS-SD (dosage of absorbent = 10 mg, C_0 = 100 mg/L, t = 5–150 min, T = 298.15 K). (b) Pseudo-first-order, (c) pseudo-second-order.

Table 3 | Kinetic constants and values of CR and MB adsorption using PS-SD

	Pseudo-first-order				Pseudo-second-order		
	q_e(exp)	q_e(cal)	k_1	R^2	q_e(cal)	k_2	R^2
CR	95.21	8.69	0.022	0.53	95.33	0.0080	0.995
MB	98.33	5.32	0.0230	0.64	99.21	0.0145	0.999

The temperature of experiments is 298.15 K.

that the adsorption of dyes was an endothermic process. The increase of temperature will increase the collision efficiency between adsorbate molecules and the adsorbent (Zhang *et al.* 2018b). This finding indicated that the adsorption of dye by PS-SD was a spontaneous process ($\Delta G^{\theta} < 0$). The positive value of ΔS^{θ} suggested that the randomness increased at the solid-solute interface during adsorption.

Table 4 | Thermodynamic parameters for the adsorption of CR and MB on PS-SD at different temperatures

	T(K)	ΔH^0(kJ/mol)	ΔS^0(J/(mol·K))	ΔG^0(kJ/mol)
MB	298.15	43.23	170.69	−7.66
	308.15			−9.37
	318.15			−11.08
CR	298.15	37.267	162.82	−11.2778
	308.15			−12.905
	318.15			−14.534

Selective adsorption

The selective adsorption performance of PS-SD on cationic dyes (MB) and anionic dyes (CR) is shown in Figure 11. Under alkaline conditions, the UV–Vis spectra of the mixture solution before and after adsorption exhibited that the absorption peaks of MB (665 nm) almost disappeared whereas the absorption peaks of CR (497 nm) almost remained at the same intensity at the same position. PS-SD selectively adsorbed the cationic dye MB. On the contrary, PS-SD selectively adsorbed the anionic dye CR under acidic conditions. After adsorption, the colour of the mixed solution was restored to red and blue (CR and MB, respectively), indicating that the dyes were selectively adsorbed on PS-SD. The possible explanation could be that the hydroxyl groups on the surface of PS-SD were easier to ionise H^+ to form O^- under alkaline conditions. In this case, the MB molecule was attracted by O^- to form monodentate complexes. However, the possible explanation could be that the amino groups on the surface of PS-SD were easier to combine H^+ to form $-NH_3^+$ under acidic condition. In this case, the CR molecule was attracted by $-NH_3^+$ to form monodentate complexes. This formation could be expressed using the following equations:

$$PS - SD - OH \Leftrightarrow PS - SD - O^- + H^+$$
$$PS - SD - O^- + MB^+ \Leftrightarrow PS - SD - O - MB \quad (7)$$

$$PS - SD - NH_2 + H^+ \Leftrightarrow PS - SD - NH_3^+$$
$$PS - SD - NH_3^+ + CR^- \Leftrightarrow PS - SD - NH_3 - CR \quad (8)$$

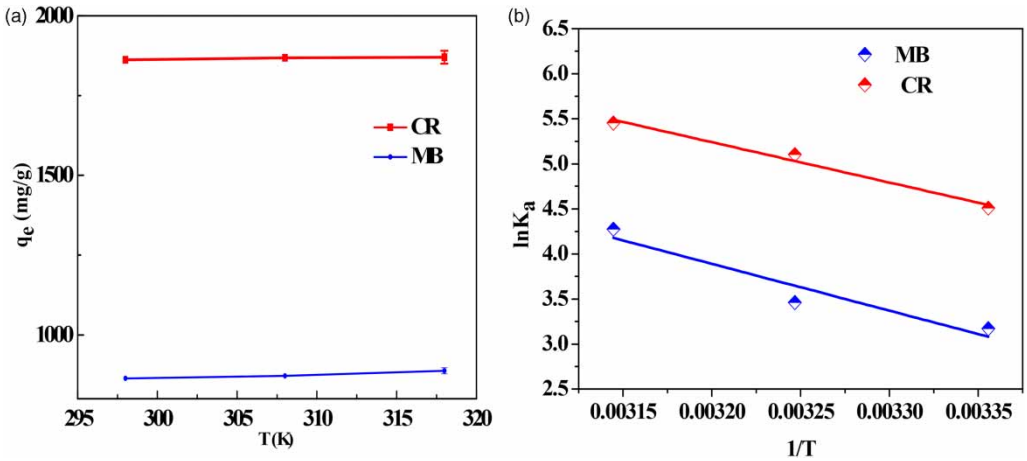

Figure 10 | Effect of temperature on the adsorption capacity of (a) CR (dosage of absorbent = 10 mg, C_0 = 2,500 mg/L, t = 150 min, T = 298.15, 308.15, and 318.15 K, pH = 5) and MB (dosage of absorbent = 10 mg, C_0 = 1,000 mg/L, t = 150 min, T = 298.15, 308.15, and 318.15 K, pH = 10), (b) thermodynamic fitting of CR and MB.

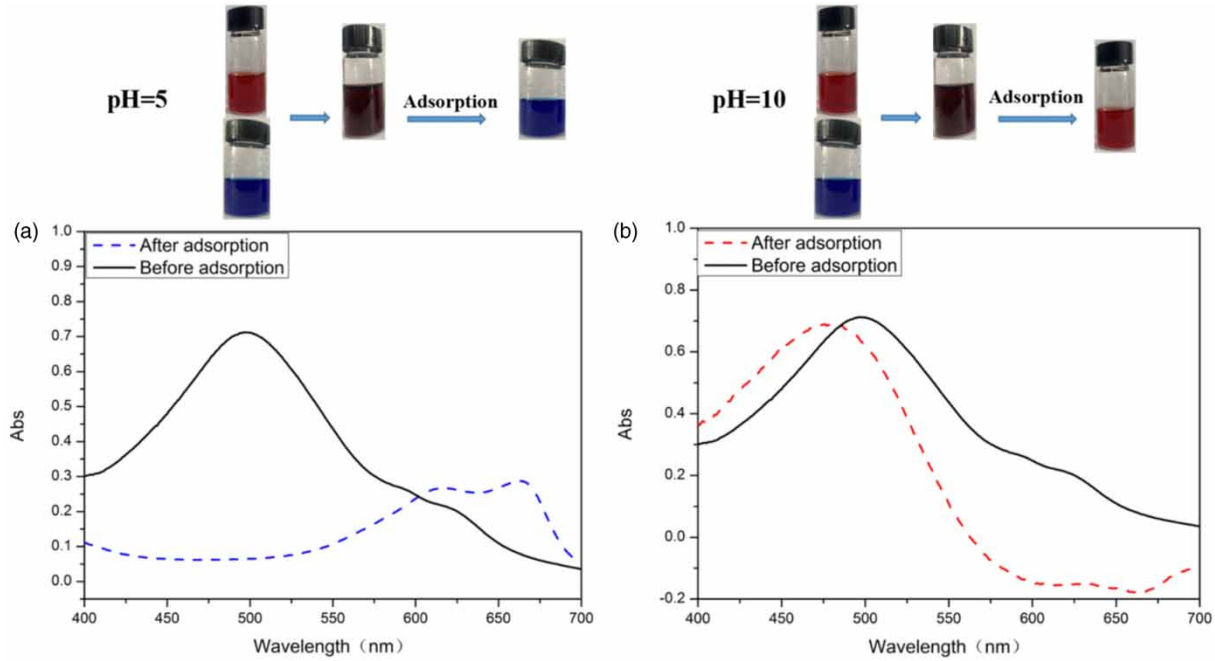

Figure 11 | Images of fast and selective adsorption, and UV-Vis spectra of the corresponding mixture before and after adsorption of (a) MB from MB/CR, (b) CR from MB/CR (dosage of absorbent = 10 mg, C_0 = 20 mg/L, t = 150 min, T = 298.15 K).

Research on recycling

The regeneration property of amide modified PS-SD for MB and CR dyes is shown in Figure 12. Two litres of CR and MB solutions were prepared with a concentration of 100 mg/L. Then 1 g of the adsorbent was added into the corresponding volumetric flask for adsorption. The adsorbed dye molecules were desorbed on the surface of PS-SD. The adsorption-desorption cycle experiment was repeated 8 times, and then each cycle was washed with ethanol for 1 h. As the number of adsorption cycles increased, the adsorption capacity of amide-modified PS-SD for MB and CR was gradually reduced, but the reduction was small. After 8 cycles of use, the adsorption capacity of amide modified PS-SD for MB removal was 88%, and the adsorption removal for CR was 85%, indicating that the amide-modified PS-SD had good recyclability.

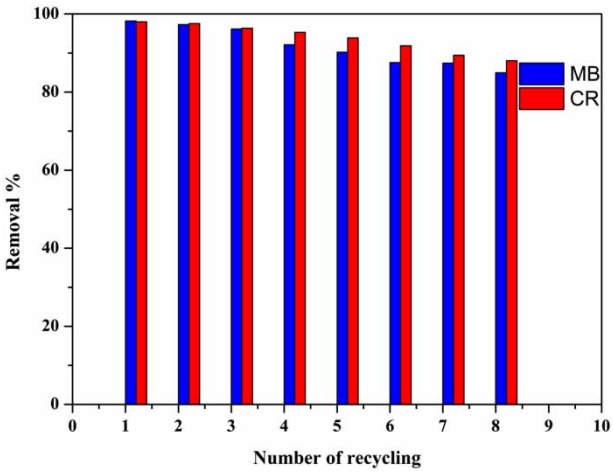

Figure 12 | Regeneration property of the PS-SD adsorbent for CR and MB dye absorption (t = 150 min, T = 298.15 K).

Adsorption mechanisms

Adsorption from solutions is a competitive process where equilibrium is determined by many factors resulting from the dye structure, textural properties, and surface chemistry of adsorbent and the specific interaction between the adsorbent surface and adsorbate. For the PS-SD adsorbent, some factors such as the surface area of the swelling and active sites, including the $-NH_3^+$ and –OH groups, played a pivotal role in the dye adsorption mechanism. To further clarify the adsorption mechanism, the FTIR spectra results were first evaluated before and after the adsorption (Figure 13). The characteristic peaks of MB is observed in the spectra of PS-SD after adsorption. The characteristic peak at around 3,380 cm^{-1} represented the stretching vibration of O-H of hydroxyl groups exhibits a slight shift to 3,405 cm^{-1} after MB adsorption, which suggests that the existence of hydrogen bond interactions between the PS-SD and MB

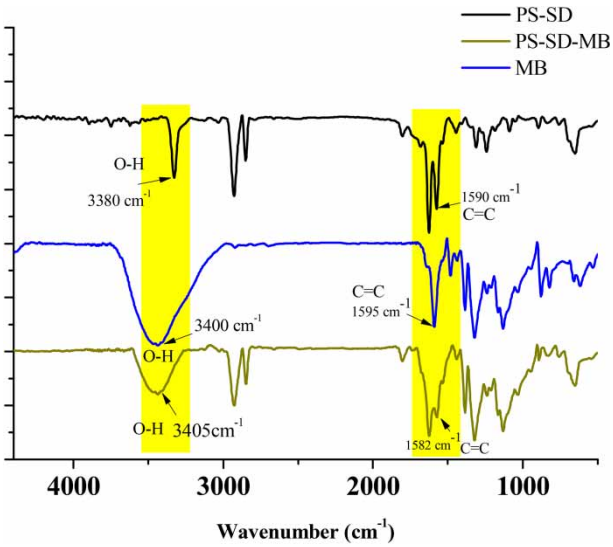

Figure 13 | FTIR spectra of PS-SD before and after the adsorption of MB.

molecules (Liu *et al.* 2019a). In addition, the characteristic peak at around 1,590 cm^{-1} that represented the stretching vibration of C = C of PS-SD exhibited a slight shift to 1,582 cm^{-1} after MB adsorption, which suggests that the existence of π-π stacking interaction and electrostatic interaction between the PS-SD and MB molecule. A reasonable mechanism by which dyes can be removed from a solution using the PS-SD adsorbent is illustrated in Figure 14.

CONCLUSION

PS-SD was synthesised from dopamine and carboxylated waste polystyrene, which was prepared by the Friedel-Crafts reaction of waste polystyrene foam and succinic anhydride. The synthesised material was porous with a considerable BET specific surface area. Under low pH conditions, the PS-SD material had a high removal capacity for CR dyes. The kinetic data of the two dyes followed the pseudo-second-order kinetics, and chemical adsorption played a leading role. Moreover, the isotherm data followed the Langmuir isotherm model. Compared with other adsorbents, the maximum adsorption capacity of amidated PS-SD for CR and MB can reach 1,880.91 and 881.62 mg/g, respectively, which showed high adsorption performance. The reusability, and high adsorption capacity of amidated PS-SD showed great application potential for the removal of dyes from wastewater.

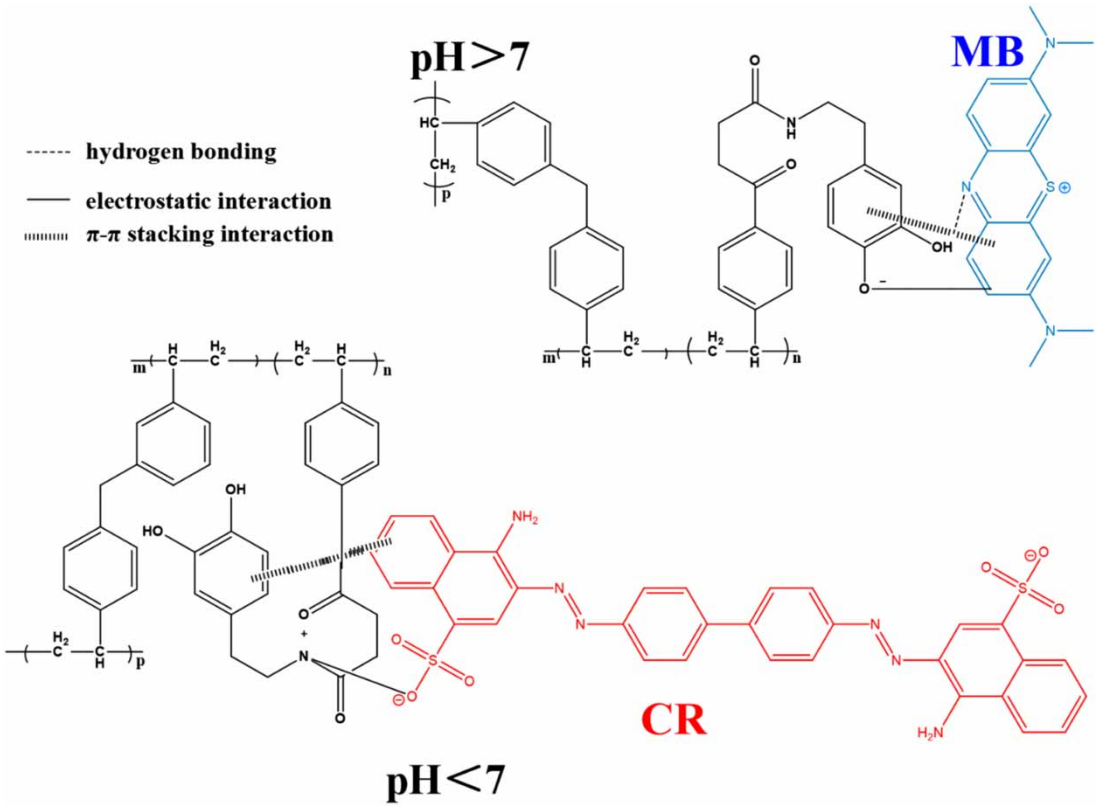

Figure 14 | Reasonable mechanisms for the adsorption of dyes onto PS-SD.

ACKNOWLEDGEMENTS

The authors thank the Sichuan Youth Science and Technology Innovation Research Team Project (No.2020JDTD0018).

DATA AVAILABILITY STATEMENT

All relevant data are included in the paper or its Supplementary Information.

REFERENCES

Ahmed, D. N., Naji, L. A., Faisal, A. A. H., Al-Ansari, N. & Naushad, M. 2020 Waste foundry sand/MgFe-layered double hydroxides composite material for efficient removal of Congo red dye from aqueous solution. *Scientific Reports* **10** (1), 2042.

Albadarin, A. B., Collins, M. N., Naushad, M., Shirazian, S., Walker, G. & Mangwandi, C. 2017 Activated lignin-chitosan extruded blends for efficient adsorption of Methylene blue. *Chemical Engineering Journal* **307**, 264–272.

Chan, S.-L., Tan, Y. P., Abdullah, A. H. & Ong, S.-T. 2016 Equilibrium, kinetic and thermodynamic studies of a new potential biosorbent for the removal of Basic Blue 3 and Congo Red dyes: pineapple (*Ananas comosus*) plant stem. *Journal of the Taiwan Institute of Chemical Engineers* **61**, 306–315.

Chaukura, N., Mamba, B. B. & Mishra, S. B. 2017 Conversion of post consumer waste polystyrene into a high value adsorbent and its sorptive properties for Congo Red removal from aqueous solution. *Journal of Environmental Management* **193**, 280–289.

Cheng, S. Y., Show, P. L., Lau, B. F., Chang, J. S. & Ling, T. C. 2019 New prospects for modified algae in heavy metal adsorption. *Trends in Biotechnology* **37** (11), 1255–12568.

Cho, E., Kim, J., Park, C. W., Lee, K. W. & Lee, T. S. 2018 Chemically bound Prussian blue in sodium alginate hydrogel for enhanced removal of Cs ions. *Journal of Hazardous Materials* **360**, 243–249.

Choi, H. Y., Bae, J. H., Hasegawa, Y., An, S., Kim, I. S., Lee, H. & Kim, M. 2020 Thiol-functionalized cellulose nanofiber membranes for the effective adsorption of heavy metal ions in water. *Carbohydrate Polymers* **234**, 115881.

Cui, W., Ji, J., Cai, Y.-F., Li, H. & Ran, R. 2015 Robust, anti-fatigue, and self-healing graphene oxide/hydrophobically associated composite hydrogels and their use as recyclable adsorbents for dye wastewater treatment. *Journal of Materials Chemistry A* **3** (33), 17445–17458.

Daneshvar, E., Vazirzadeh, A., Niazi, A., Kousha, M., Naushad, M. & Bhatnagar, A. 2017 Desorption of Methylene blue dye from brown macroalga: effects of operating parameters, isotherm study and kinetic modeling. *Journal of Cleaner Production* **152**, 443–453.

Dardouri, M., Ammari, F., BelHadj Amor, A. & Meganem, F. 2018 Adsorption of cadmium (II), zinc (II) and iron (III) from water by new cross-linked reusable polystyrene adsorbents. *Materials Chemistry and Physics* **216**, 435–445.

Dinari, M., Shirani, M. A., Maleki, M. H. & Tabatabaeian, R. 2020 Green cross-linked bionanocomposite of magnetic layered double hydroxide/guar gum polymer as an efficient adsorbent of Cr(VI) from aqueous solution. *Carbohydrate Polymers* **236**, 116070.

Duan, M., Ma, J. & Fang, S. 2019 Synthesis of hydrazine-grafted guar gum material for the highly effective removal of organic dyes. *Carbohydrate Polymers* **211**, 308–314.

Gao, X., Li, M., Zhao, Y. & Zhang, Y. 2019 Mechanistic study of selective adsorption of Hg^{2+} ion by porous alginate beads. *Chemical Engineering Journal* **378**, 122096.

Han, H., Rafiq, M. K., Zhou, T., Xu, R., Masek, O. & Li, X. 2019 A critical review of clay-based composites with enhanced adsorption performance for metal and organic pollutants. *Journal of Hazardous Materials* **369**, 780–796.

Ji, Y., Wen, Y., Wang, Z., Zhang, S. & Guo, M. 2020 Eco-friendly fabrication of a cost-effective cellulose nanofiber-based aerogel for multifunctional applications in Cu(II) and organic pollutants removal. *Journal of Cleaner Production* **255**, 120276.

Kumari, S., Mankotia, D. & Chauhan, G. S. 2016 Crosslinked cellulose dialdehyde for Congo red removal from its aqueous solutions. *Journal of Environmental Chemical Engineering* **4** (1), 1126–1136.

Lau, H. H., Yakovlev, N. L., Ooi, C. P. & Kiryukhin, M. V. 2018 Adsorption kinetics of tannic acid onto an albumin-terminated multilayer thin films. *Colloid and Polymer Science* **297** (3), 417–422.

Lei, Z., Gao, W., Zeng, J., Wang, B. & Xu, J. 2020 The mechanism of Cu (II) adsorption onto 2,3-dialdehyde nano-fibrillated celluloses. *Carbohydrate Polymers* **230**, 115631.

Li, L., Zhao, J., Sun, Y., Yu, F. & Ma, J. 2019 Ionically cross-linked sodium alginate/κ-carrageenan double-network gel beads with low-swelling, enhanced mechanical properties, and excellent adsorption performance. *Chemical Engineering Journal* **372**, 1091–1103.

Li, D., Tian, X., Wang, Z., Guan, Z., Li, X., Qiao, H., Ke, H., Luo, L. & Wei, Q. 2020 Multifunctional adsorbent based on metal-organic framework modified bacterial cellulose/chitosan composite aerogel for high efficient removal of heavy metal ion and organic pollutant. *Chemical Engineering Journal* **383**, 123127.

Lin, D., Shi, M., Zhang, Y., Wang, D., Cao, J., Yang, J. & Peng, C. 2019 3D crateriform and honeycomb polymer capsule with nano re-entrant and screen mesh structures for the removal of multi-component cationic dyes from water. *Chemical Engineering Journal* **375**, 121911.

Liu, Z., Xu, D., Zhao, X., Xia, N., Yang, G., Fatehi, P., Kong, F. & Wang, S. 2018 Preparation and application of carboxymethylated xylan as a flocculant for ethyl violet dye in aqueous systems. *Journal of Wood Chemistry and Technology* **38** (4), 324–337.

Liu, X., Tian, J., Li, Y., Sun, N., Mi, S., Xie, Y. & Chen, Z. 2019a Enhanced dyes adsorption from wastewater via Fe_3O_4 nanoparticles functionalized activated carbon. *Journal of Hazardous Materials* **373**, 397–407.

Liu, Y., Wang, R., Bai, J., Jiao, T., Bai, Z., Zhang, L., Zhang, Q., Zhou, J. & Peng, Q. 2019b Non-covalent self-assembly of multi-target polystyrene composite adsorbent with highly

efficient Cu(II) ion removal capability. *Colloids and Surfaces A: Physicochemical and Engineering Aspects* **577**, 674–682.

Liu, Y., Huang, J., Xu, H., Zhang, Y., Hu, T., Chen, W., Hu, H., Wu, J., Li, Y. & Jiang, G. 2020a A magnetic macro-porous biochar sphere as vehicle for the activation and removal of heavy metals from contaminated agricultural soil. *Chemical Engineering Journal* **390**, 124638.

Liu, Y., Liu, L., Wang, K., Zhang, H., Yuan, Y., Wei, H., Wang, X., Duan, Y., Zhou, L. & Zhang, J. 2020b Modified ammonium persulfate oxidations for efficient preparation of carboxylated cellulose nanocrystals. *Carbohydrate Polymers* **229**, 115572.

Ma, M., Ying, H., Cao, F., Wang, Q. & Ai, N. 2020 Adsorption of Congo red on mesoporous activated carbon prepared by CO_2 physical activation. *Chinese Journal of Chemical Engineering* **28** (4), 1069–1076.

Naushad, M., Abdullah Alothman, Z., Rabiul Awual, M., Alfadul, S. M. & Ahamad, T. 2015 Adsorption of rose Bengal dye from aqueous solution by amberlite Ira-938 resin: kinetics, isotherms, and thermodynamic studies. *Desalination and Water Treatment* **57** (29), 13527–13533.

Naushad, M., Sharma, G. & Alothman, Z. A. 2019 Photodegradation of toxic dye using Gum Arabic-crosslinked-poly(acrylamide)/$Ni(OH)_2$/FeOOH nanocomposites hydrogel. *Journal of Cleaner Production* **241**, 118263.

Qiao, L., Li, S., Li, Y., Liu, Y. & Du, K. 2020 Fabrication of superporous cellulose beads via enhanced inner cross-linked linkages for high efficient adsorption of heavy metal ions. *Journal of Cleaner Production* **253**, 120017.

Roy, C., Dutta, A., Mahapatra, M., Karmakar, M., Roy, J. S. D., Mitra, M., Chattopadhyay, P. K. & Singha, N. R. 2019 Collagenic waste and rubber based resin-cured biocomposite adsorbent for high-performance removal(s) of Hg(II), safranine, and brilliant cresyl blue: a cost-friendly waste management approach. *Journal of Hazardous Materials* **369**, 199–213.

Satheshkumar, M., Anand, B., Muthuvel, A., Rajarajan, M., Mohana, V. & Sundaramanickam, A. 2020 Enhanced photocatalytic dye degradation and antibacterial activity of biosynthesized ZnO-NPs using curry leaves extract with coconut water. *Nanotechnology for Environmental Engineering* **5** (3), 1–11.

Sharif, F., Gagnon, L. R., Mulmi, S. & Roberts, E. P. 2017 Electrochemical regeneration of a reduced graphene oxide/magnetite composite adsorbent loaded with Methylene blue. *Water Research* **114**, 237–245.

Sharma, G., Kumar, A., Sharma, S., Naushad, M., Dhiman, P., Vo, D.-V. N. & Stadler, F. J. 2020 Fe_3O_4/ZnO/Si_3N_4 nanocomposite based photocatalyst for the degradation of dyes from aqueous solution. *Materials Letters* **278**, 128359.

Tran, H. N., You, S. J., Hosseini-Bandegharaei, A. & Chao, H. P. 2017 Mistakes and inconsistencies regarding adsorption of contaminants from aqueous solutions: a critical review. *Water Research* **120**, 88–116.

Unnikrishnan, S., Khan, M. H. & Ramalingam, K. 2018 Dye-tolerant marine *Acinetobacter baumannii*-mediated biodegradation of reactive red. *Water Science and Engineering* **11** (4), 265–275.

Wan, X., Zhan, Y., Long, Z., Zeng, G. & He, Y. 2017 Core@double-shell structured magnetic halloysite nanotube nano-hybrid as efficient recyclable adsorbent for Methylene blue removal. *Chemical Engineering Journal* **330**, 491–504.

Wang, H., Zhou, P., Wang, J., Wang, Y., Wei, J., Zhan, H., Guo, R. & Zhang, Y. 2018a Synthesis and characterization of Rectorite/ZnO/TiO_2 composites and their properties of adsorption and photocatalysis for the removal of Methylene Blue dye. *Journal of Wuhan University of Technology-Mater. Sci. Ed.* **33** (3), 729–735.

Wang, J., Wang, L., Xu, C., Zhi, R., Miao, R., Liang, T., Yue, X., Lv, Y. & Liu, T. 2018b Perfluorooctane sulfonate and perfluorobutane sulfonate removal from water by nanofiltration membrane: the roles of solute concentration, ionic strength, and macromolecular organic foulants. *Chemical Engineering Journal* **332**, 787–797.

Wang, X.-L., An, W.-L., Yang, Y., Hu, Z.-Y., Xu, S., Liao, W. & Wang, Y.-Z. 2019 Porous gel materials from waste thermosetting unsaturated polyester for high-efficiency wastewater treatment. *Chemical Engineering Journal* **361**, 21–30.

Wang, Z., Yao, M., Wang, X., Li, S., Liu, Y. & Yang, G. 2020 Influence of reaction media on synthesis of dialdehyde cellulose/GO composites and their adsorption performances on heavy metals. *Carbohydrate Polymers* **232**, 115781.

Wu, Z., Deng, W., Zhou, W. & Luo, J. 2019 Novel magnetic polysaccharide/graphene oxide @Fe_3O_4 gel beads for adsorbing heavy metal ions. *Carbohydrate Polymers* **216**, 119–128.

Wu, Q., He, H., Zhou, H., Xue, F., Zhu, H., Zhou, S., Wang, L. & Wang, S. 2020 Multiple active sites cellulose-based adsorbent for the removal of low-level Cu(II), Pb(II) and Cr(VI) via multiple cooperative mechanisms. *Carbohydrate Polymers* **233**, 115860.

Xi, C., Wang, R., Rao, P., Zhang, W., Yan, L., Li, G., Chai, F., Cai, Y., Luo, T. & Zhou, X. 2020 The fabrication and arsenic removal performance of cellulose nanocrystal-containing absorbents based on the 'bridge joint' effect of iron ions. *Carbohydrate Polymers* **237**, 116129.

Yang, S., Wang, L., Zhang, X., Yang, W. & Song, G. 2015 Enhanced adsorption of Congo red dye by functionalized carbon nanotube/mixed metal oxides nanocomposites derived from layered double hydroxide precursor. *Chemical Engineering Journal* **275**, 315–321.

Zhang, H. Q., Zhang, T. T., Tian, L., Qu, J. Y., Liu, P. G., Wang, X. M. & Zhang, X. 2018a Amino-modified hierarchically macro-mesoporous cross-linked polystyrene: a novel adsorbent for removal of salicylic acid from aqueous solution. *Journal of the Taiwan Institute of Chemical Engineers* **88**, 186–192.

Zhang, W., Deng, Q., He, Q., Song, J., Zhang, S., Wang, H., Zhou, J. & Zhang, H. 2018b A facile synthesis of core-shell/bead-like poly (vinyl alcohol)/alginate@PAM with good adsorption capacity, high adaptability and stability towards Cu(II) removal. *Chemical Engineering Journal* **351**, 462–472.

First received 7 February 2021; accepted in revised form 24 March 2021. Available online 2 April 2021